

On the Modelling of Rate-Dependent Domain Switching in Piezoelectric Materials under Superimposed Stresses

A. Arockiarajan¹ and A. Menzel²

Abstract: To study rate-dependent properties of piezoelectric materials a micro-mechanically motivated model is applied in this work. The developed framework is embedded into a coupled three-dimensional finite element setting, whereby each element is assumed to represent one grain and, moreover, possesses a random initialisation of the underlying polarisation direction. Furthermore, an energy-based criterion is used for the initiation of the onset of domain switching and the subsequent propagation of domain wall motion during the switching process is modelled via a linear kinetics theory. The interaction between individual grains is thereby incorporated by means of a probabilistic approach – a purely phenomenologically motivated concept. To study the overall bulk ceramics behaviour, straightforward volume-averaging techniques are applied. In addition, rate-dependent properties under cyclic electrical loading combined with mechanical loads at various frequencies are studied, whereby use of a so-called volume fraction concept is made. The proposed model provides further insights into rate-dependent behaviour as experimentally observed and reported in the literature.

Keyword: piezoelectricity, rate-dependency, linear kinetics theory, electro-mechanical loading, coupled finite element formulation

1 Introduction

In recent years, the study and application of advanced materials plays an increasingly important role for designing structures, intelligent systems,

micro-electromechanical systems and so forth. Smart materials thereby turn out to be of special interest since they serve as elementary (linear) components such as sensors and actuators. Electro-active ceramic materials – for instance piezoelectrics, ferroelectrics and electrostrictors – are nowadays widely used for these components. An overview on common application, for instance active damping, vibration suppression, noise control, precision positioning, and so forth is given in Uchino (1997). Most of these applications benefit from controlling large mechanical forces and reasonable high strains according to the application of rather high stresses and electric fields. At high electro-mechanical loading levels, however, the electro-active ceramics of interest exhibit strongly nonlinear response. Such domain switching effects, stemming from reorientation of the underlying polarisation directions with respect to the applied loading directions, play a vital role for the operation of these materials. Accordingly, it is of cardinal importance to account for this characteristic constitutive behaviour within sound modelling approaches of related smart structures and devices. Various experimental investigations on the nonlinear response of these materials have been reported in the literature. Commonly, such studies are carried out on a sample specimen which is subjected to cyclic electrical and / or mechanical loading and related observations are referred to the overall macroscopic behaviour. As a key result from these elaborations, parameter variations such as composition effects, the influence of phase change, macroscopic creep effects, etc. can be studied for hard and soft piezoelectric materials. For further details, the reader is referred to the contributions by Cao and Evans (1993), Hwang, Lynch, and McMeeking (1995), Lynch (1996), Lu, Fang, Li, and Hwang (1999),

¹Department of Applied Mechanics, Indian Institute of Technology Madras, 600036 Chennai, India

²Department of Mechanical Engineering, Institute of Mechanics and Control Engineering, Chair of Continuum Mechanics, University of Siegen, Germany

Fang and Li (1999), Huber and Fleck (2004) as well as to the monographs by Lupascu (2004) and Smith (2005).

To further study the nonlinear behaviour of piezoelectric materials, theoretical modelling approaches have been proposed which allow classification into two different categories: On the one hand, various phenomenological or rather macro-mechanically motivated formulations have been developed. So-called internal state variables are thereby embedded into representative functions and constitutive equations. By analogy with for instance J_2 plasticity, where the effects of plastic slide are accounted for on a macro-level rather than modelling the onset and movement of dislocations on a micro-level, such approaches capture purely macroscopic response of piezoelectric materials. Nevertheless, important insight into the design and interpretation of experiments as well as the overall behaviour of these materials can be provided. As a side aspect, thermodynamic relations are commonly fulfilled within these approaches. A comprehensive model was developed in, e.g., Bassiouny, Ghaleb, and Maugin (1988a,b), wherein the polarisation serves as an internal state variable. Furthermore, a free energy function is established which, in addition to the polarisation, depends on strains and temperature. Similar modelling concepts, as based on irreversible polarisation vectors and irreversible strains as internal state variables, are reported in the literature; see for instance Lynch and McMeeking (1994), Kamlah and Tsakmakis (1999), Landis (2002), Elhadrouz, Zineb, and Patoor (2005), or Schröder and Romanowski (2005). On the other hand, different micro-mechanically motivated modelling approaches have been proposed. The constitutive relation of these formulations often directly address physical aspects of the material behaviour combined with energy-based domain switching criteria. Different length scales might thereby come into the picture and the overall poly-crystalline response is usually incorporated via appropriate averaging techniques; the reader is referred to Hwang and McMeeking (1998b), Chen and Lynch (1998), Lu, Fang, Li, and Hwang (1999) or Srivastava and Weng

(2006). Hwang and McMeeking (1998b) proposed a switching criterion, wherein the sum of work performed under mechanical and electrical loading is considered as a driving force for switching whenever a critical energy barrier is exceeded. Chen and Lynch (1998) established a switching criterion by means of an internal variable approach combined with a volume fraction concept in order to represent the assembly of various domains, see also the contribution by Sun and Achuthan (2004) for an internal variable based switching formulation. A criterion which enables to trigger switching if the reduction in potential energy related to a starting and an ending state exceeds a critical energy threshold was developed by Hwang and McMeeking (1998a). Recently, Srivastava and Weng (2006) published a dual-phase homogenisation theory, wherein the reduction in Gibbs free energy serves as the driving force for domain switching.

Nowadays, commercialised applications of smart structures and materials perform under various loading levels as well as under different loading frequencies. Accordingly, there is a need to include rate-dependent effects into the modelling of the non-linear response of piezoelectric materials. More than fifty years ago, Merz (1954) experimentally investigated the dependency of the electric field and the temperature on the switching time and the switching current. As a result, a reduction of the switching process time and consequently an increase in the switching current has been observed for increasing temperature but constant electric field. Viehland and Chen (2000) published experimental results on frequency-dependent characteristics such as for instance that the polarisation effect increases at higher loading frequencies even though the electric field decreases. Detailed experimental studies have been performed by Zhou, Kamlah, and Munz (2001), whereby a quasi-static frequency range between 0.1 Hz to 1.0 Hz has been considered. It thereby turned out that the coercive electric field increases and that the remanent polarisation decreases for increasing loading frequencies. A related theoretical model, by means of exponential functions with respect to the applied

electric field level and the loading frequency, was developed by Landauer, Young, and Drougard (1956). Omura, Adachi, and Ishibashi (1991) established a formulation, wherein the delay during the switching process is accounted for by a viscosity constant which leads to a change in the coercive field. Abeyaratne, Kim, and Knowles (1994) developed a constitutive model for domain switching and nucleation effects based on a phase transition approach motivated by a thermal activation theory. Kim and Jiang (2002) published a related finite element formulation and proposed a domain (switching) nucleation and propagation framework by means of a (continuous) volume fraction evolution approach. For further background information the reader is referred to the contributions by, e.g., Janta (1971) or Arlt (1996a,b, 1997).

The present paper deals with an energy-based micro-mechanically motivated non-linear model combined with a probabilistic approach. Moreover, the applied model is embedded into a three-dimensional coupled finite element formulation. Rate-dependency is captured via a linear kinetics theory, compare Arlt (1996a,b, 1997). The main features of the present work are: (i) domain switching is initiated as soon as the reduction in Gibbs free energy exceeds a critical energy barrier; (ii) interaction effects between individual grains is modelled via a phenomenological probabilistic approach by weighting the introduced energy barrier with an energy-related polynomial factor; (iii) nucleation and propagation of domain walls during the switching process is captured using a linear kinetics theory. To realistically capture rate-dependencies, a limit time parameter for domain switching is introduced – a non-constant parameter which depends on the applied electric field, mechanical stresses, and so forth; (iv) the adopted framework is embedded into a coupled finite element formulation, whereby a straightforward staggered iteration scheme is applied – to be specific, a sequence of linear problems is solved for within each and every loading-/time step. Individual finite elements are thereby equipped with initially random polarisation orientation; (v) the examples

investigated in this contribution extend our previous work, compare Arockiarajan, Delibas, Menzel, and Seemann (2006); Arockiarajan, Menzel, Delibas, and Seemann (2006a,b), by placing emphasis on various loading conditions applied to a representative specimen, namely cyclic electrical loading at different frequencies together with superimposed axial and lateral mechanical stresses.

The outline of the paper is as follows: essential balance relations and constitutive equations are summarised in section 2. The adopted energy-based switching criterion is discussed in section 3 where in addition the underlying basics of the applied rate-dependent switching theory as well as the modelling of intergranular effects by means of a probabilistic approach are outlined. The finite-element-based simulation technique and numerical examples are highlighted in section 4. Finally, the paper is concluded with a short summary in section 5.

2 Constitutive modelling

Piezoelectric materials possess a pronounced micro-structure as represented by the underlying lattice structures and, moreover, exhibit strongly temperature-dependent response. While these materials embody cubic symmetry above the Curie temperature, the so-called paraelectric phase, we are mainly interested in the modelling of ferroelectric phases. Accordingly, phase-transformations or rather switching effects, which results in so-called spontaneous polarisation and spontaneous strains, come into the picture, whereby we restrict ourselves to tetragonal symmetry. In this regard, essential balance and constitutive equations are reviewed in the following.

2.1 Balance equations

Consider a continuum body B represented by its configuration $\mathcal{B} \subset \mathfrak{R}^3$ with placements $\mathbf{x} \in \mathfrak{R}^3$. As essential degrees of freedom we consider the electric potential $\phi \in \mathfrak{R}$ and the displacement field $\mathbf{u} \in \mathfrak{R}^3$. Consequently, balance of linear momentum for the static case and the Gauß equation take

the well-established format

$$\begin{aligned} \mathbf{0} &= \nabla \cdot \boldsymbol{\sigma} + \mathbf{b} && \text{in } \mathcal{B} \\ \mathbf{u} &= \mathbf{u}^p && \text{on } \partial\mathcal{B}_u \\ \mathbf{t} &= \mathbf{t}^p = \boldsymbol{\sigma} \cdot \mathbf{n}_\sigma && \text{on } \partial\mathcal{B}_\sigma \end{aligned} \quad (1)$$

together with

$$\begin{aligned} 0 &= \nabla \cdot \mathbf{D} - \rho_f && \text{in } \mathcal{B} \\ \phi &= \phi^p && \text{on } \partial\mathcal{B}_\phi \\ -q &= -q^p = \mathbf{D} \cdot \mathbf{n}_D && \text{on } \partial\mathcal{B}_D \end{aligned} \quad (2)$$

whereby $\partial\mathcal{B}_u \cup \partial\mathcal{B}_\sigma = \partial\mathcal{B}_\phi \cup \partial\mathcal{B}_D = \partial\mathcal{B}$ and $\partial\mathcal{B}_u \cap \partial\mathcal{B}_\sigma = \partial\mathcal{B}_\phi \cap \partial\mathcal{B}_D = \emptyset$. Adopting standard notation, $\boldsymbol{\sigma}$ denotes the stress tensor, \mathbf{D} represents the electric displacement vector, and $\mathbf{n}_{\sigma,D}$ characterise unit normal vectors with respect to the corresponding surfaces.

2.2 Constitutive equations

The so-called nonlinear representation of the constitutive equations for $\boldsymbol{\sigma}$ and \mathbf{D} account for spontaneous strains $\boldsymbol{\varepsilon}^s = \boldsymbol{\varepsilon}^s [3\mathbf{m} \otimes \mathbf{m} - \mathbf{I}]/2$ as well as for spontaneous polarisation $\mathbf{P}^s = P^s \mathbf{m}$ with $\|\mathbf{m}\| = 1$, namely

$$\boldsymbol{\sigma} = \mathbf{C} : [\boldsymbol{\varepsilon} - \boldsymbol{\varepsilon}^s] - \mathbf{d} \cdot \mathbf{E} \quad (3)$$

$$\mathbf{D} = \mathbf{d} : [\boldsymbol{\varepsilon} - \boldsymbol{\varepsilon}^s] + \mathbf{k} \cdot \mathbf{E} + \mathbf{P}^s \quad (4)$$

wherein $\boldsymbol{\varepsilon} = \nabla^{\text{sym}} \mathbf{u}$ and $\mathbf{E} = -\nabla\phi$ denote the total strain tensor and the electric field, respectively, compare Jaffe, Cook, and Jaffe (1971). Both, the elastic constant \mathbf{C} as well as the dielectric permittivity \mathbf{k} are assumed to reflect isotropic response so that three material parameters must be considered – for instance the two Lamé parameters λ , μ and k which, by weighting the second order identity, determines \mathbf{k} . Experimental investigations reported in Hwang, Lynch, and McMeeking (1995) show that the material symmetry should be reflected at least by the dielectric third order tensor \mathbf{d} . Moreover, the properties of this quantity might vary between different domains. Since we are particularly interested in the modelling of perovskite crystallites with tetragonal microstructure, the transversely isotropic representation

$$\begin{aligned} \mathbf{d} &= d_{33} \mathbf{M} + d_{31} [\mathbf{m} \otimes \mathbf{I} - \mathbf{M}] \\ &\quad + d_{15} \left[\frac{1}{2} [\mathbf{I} \otimes \mathbf{m} + \mathbf{I} \overline{\otimes} \mathbf{m}] - \mathbf{M} \right] \end{aligned} \quad (5)$$

is adopted in the following; see Kamlah (2001) for a detailed review on the underlying material symmetry relations. For notational convenience the abbreviations $\mathbf{M} = \mathbf{m} \otimes \mathbf{m} \otimes \mathbf{m}$ and $[\mathbf{I} \otimes \mathbf{m} + \mathbf{I} \overline{\otimes} \mathbf{m}] : \mathbf{a} = [\mathbf{I} \otimes \mathbf{m} + \mathbf{I} \overline{\otimes} \mathbf{m}] : \mathbf{a}^\dagger$ for all second order tensors \mathbf{a} , whereby \bullet^\dagger denotes transposition, have been introduced in eq.(5).

The numerical computations discussed as this work proceeds consider specimens which, from a macroscopic point of view, are initially isotropic. To account for this un-poled virgin state, a random orientation is applied to the underlying unit-cells by means of Eulerian angles from which local spontaneous polarisation vectors and spontaneous strain tensors are determined. For details of implementation and further background information the reader is refer to our previous works Arockiarajan, Menzel, Delibas, and Seemann (2006a,b) and the monograph by Goldstein, Poole, and Safko (2002).

3 Modelling of domain switching processes

The macroscopic nonlinear behaviour of polycrystalline piezoelectric materials mainly stems from phase-transformation phenomena on related micro-scales. Such domain switching effects are commonly identified with a reorientation of polarisation vectors or rather a reorientation of the underlying unit-cells. In the following, perovskite crystallites with tetragonal microstructure are elaborated so that solely 90° or 180° domain switching occurs; see figure 1 for a graphical representation. For a particular finite time interval $\Delta t = t_{n+1} - t_n > 0$ of interest polarisation vectors might either reorient according to one out of four possible 90° switching directions or align with respect to a 180° switching processes. Next, related modelling concepts are briefly reviewed.

3.1 Energy-based switching criterion

An energy-based switching criterion as advocated by, McMeeking and Hwang (1997) is applied in this work. In this regard, switching is initiated as soon as the related reduction in energy (ΔU) exceeds a critical possibly constant value $\Delta\psi_c$,

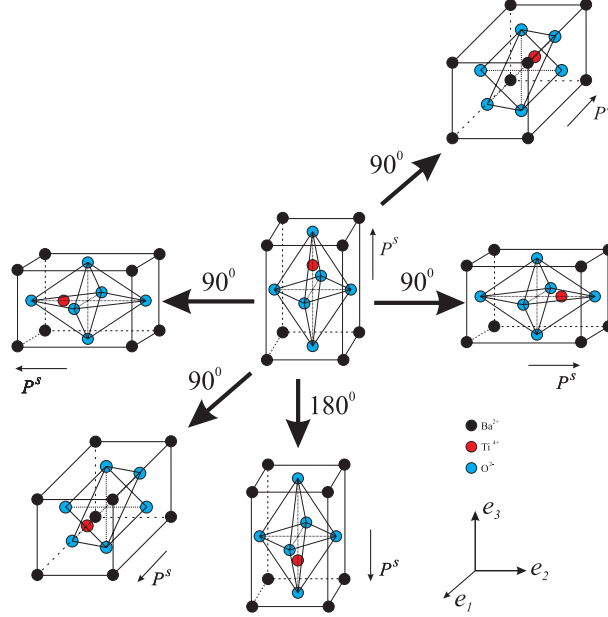


Figure 1: Different types of 90° and 180° domain switching for a representative tetragonal lattice structure.

namely

$$\Delta U(\mathbf{u}, \phi) + \Delta \psi_c \leq 0. \quad (6)$$

Following Hwang, Lynch, and McMeeking (1995), we adopt the particular format

$$\Delta U = -\mathbf{E} \cdot \Delta \mathbf{P}^s - \boldsymbol{\sigma} : \Delta \boldsymbol{\varepsilon}^s \quad \text{together with} \quad (7)$$

$$\Delta \psi_c = 2 E_0 P_0, \quad (8)$$

wherein $\Delta \mathbf{P}^s$ and $\Delta \boldsymbol{\varepsilon}^s$ denote the change in spontaneous polarisation and strains, respectively, while $E_0 > 0$ and $P_0 > 0$ characterise the coercive electric field value and the polarisation parameter. Taking a specific load step into account, the domain of interest might meet this switching criterion for several polarisation directions. For the numerical examples highlighted in the sequel, the phase-transformations realised are referred to polarisation directions which render the largest (local) energy reduction value.

3.2 Time-dependent nucleation and propagation

Experimental observations show that piezoelectric materials exhibit also time- or rather rate-dependent response since domain switching processes in general require a finite interval of time

to be completed. In the following, the modelling of such rate-dependent domain switching process is triggered by using the previously highlighted switching criterion. Subsequently, a so-called volume fraction concept combined with a linear kinetics theory is adopted, in this work; for detailed discussions see also previous elaborations reported in Delibas, Arockiarajan, and Seemann (2006) and Arockiarajan, Delibas, Menzel, and Seemann (2006); Arockiarajan, Menzel, Delibas, and Seemann (2006a). In this regard, eqs.(6, 7, 8) are supplemented by a critical switching (limit) time Δt_l which is assumed to depend on the individual loading level, namely

$$\Delta t_l = \frac{C_1}{\|\mathbf{E}\|} + \frac{C_2}{\|\boldsymbol{\sigma}\|}, \quad (9)$$

whereby the constitutive parameters $C_1, C_2 > 0$ might themselves depend on temperature, the size of the domain, and so forth; compare Merz (1954). Practically speaking, Δt_l represents the time interval required to complete a switching process. When considering a sufficiently large load step related to a time increment $\Delta t < \Delta t_l$, the updated polarisation direction should, accordingly, not correspond to the fully switched state. In this regard, a simple volume fraction concept in terms of the parameter τ – representing the frac-

tion between the time elapsed since the switching process has been initiated for a particular loading level and the critical switching (limit) time – is applied. The modified update scheme consequently results in

$$\mathbf{P}_{n+1}^s = \tau \tilde{\mathbf{P}}_{n+1}^s + [1 - \tau] \mathbf{P}_n^s \quad \text{and} \quad (10)$$

$$\boldsymbol{\varepsilon}_{n+1}^s = \tau \tilde{\boldsymbol{\varepsilon}}_{n+1}^s + [1 - \tau] \boldsymbol{\varepsilon}_n^s, \quad (11)$$

wherein $\tilde{\mathbf{P}}_{n+1}^s$ and $\tilde{\boldsymbol{\varepsilon}}_{n+1}^s$ represent the fully switched state. For surveys on alternative modelling approaches the reader is referred to Smith and Ounates (2000) and Kim and Seelecke (2007) as well as to the investigations by Liu and Lynch (2006), and to references cited in these works.

3.3 Grain boundary effects

So-called grain boundary effects crucially affect the overall response of poly-crystalline piezoelectric materials. To give but a few examples, high local loading levels and micro-cracking might occur. The model discussed until here allows switching, as initiated by the criterion (7, 8), in the region of interest without directly incorporating any additional influences of the neighbouring material. In this regard and in view of related finite element applications one could either deal with very fine meshes, covering representative geometries combined with advanced modelling strategies for the grain boundaries themselves, or incorporate such grain boundary effects on a phenomenological or rather constitutive level. Practically speaking and with respect to comparisons of simulations with experimental investigations, both approaches should render hysteresis and butterfly curves which do not possess sharp corners near to the critical electric field value; compare figure 3. In the following we pursue along the lines of the latter framework and, in order to take such grain boundary effects into account, introduce a phenomenologically motivated probability function P into the switching criterion, to be specific

$$P = \begin{cases} \left[\frac{-\Delta\bar{U}}{2E_0P_0} \right]^p & \text{for } -\Delta\bar{U} < 2E_0P_0 \\ 1 & \text{for } -\Delta\bar{U} \geq 2E_0P_0 \end{cases} \quad (12)$$

wherein $-\Delta\bar{U} = \bar{\mathbf{E}}^e \cdot \Delta\mathbf{P}^{se} + \bar{\boldsymbol{\sigma}}^e : \Delta\boldsymbol{\varepsilon}^{se}$ and the parameter $p \geq 0$ allows calibration of simulation results with experimental data. Moreover, volume-averaged quantities have been introduced in view of the underlying domains, i.e. $\bar{\mathbf{E}}^e = \frac{1}{V^e} \int_{V^e} \mathbf{E}^e \, \gamma$ and $\bar{\boldsymbol{\sigma}}^e = \frac{1}{V^e} \int_{V^e} \boldsymbol{\sigma}^e \, \gamma$. As such, the finally applied switching criterion results in

$$\bar{\mathbf{E}}^e \cdot \Delta\mathbf{P}^{se} + \bar{\boldsymbol{\sigma}}^e : \Delta\boldsymbol{\varepsilon}^{se} > 2E_0P_0P. \quad (13)$$

Please note that the incorporation of any suitable, for example statistically motivated, probability function is straightforward.

4 Numerical examples

The previously highlighted framework has been embedded into a coupled finite element formulation with \mathbf{u} and ϕ constituting the underlying degrees of freedom. Both, spontaneous polarisation \mathbf{P}^s as well as spontaneous strains $\boldsymbol{\varepsilon}^s$ are thereby introduced as so-called internal variables stored at the integration point level or, for the problem at hand, at the element level. For detailed background information the reader is referred to Allik and Hughes (1970), Gaudenzi and Bathe (1995), or Schröder and Gross (2004) among others.

As a first step towards detailed discretisation techniques, homogenisation schemes, and more advanced simulations we assume that every individual finite element (Q1Q1) represents one grain and thereby do not distinguish between grains and domains; see figure 2 for a graphical illustration.

As discussed in section 2.2, the initial polarisation direction of each finite element is randomly generated by means of Eulerian angles so that the initial macroscopic state monitors the response of an un-poled ceramics. Thereafter, a simple staggered iteration technique is applied within each load step to incorporate switching effects:

(I) based on the coupled finite element formulation, compute \mathbf{u} and ϕ at fixed \mathbf{P}^s , $\boldsymbol{\varepsilon}^s$, and \mathbf{d} for given boundary and loading conditions

(II) based on the switching criterion, compute \mathbf{P}^s , $\boldsymbol{\varepsilon}^s$, and \mathbf{d} at fixed \mathbf{u} and ϕ

- (III) based on the coupled finite element formulation, recompute \mathbf{u} and ϕ at fixed \mathbf{P}^s , $\boldsymbol{\varepsilon}^s$, and \mathbf{d} for given boundary and loading conditions

Further details are provided in Arockiarajan, Menzel, Delibas, and Seemann (2006a,b). Please note that steps (II) and (III) can be repeated until a suitable convergence criterion is met. In view of the numerical examples elaborated in this work, however, it turned out that sufficiently accurate results could be obtained without taking a related (additional) iteration scheme into account. The subsequent sections address the simulation of a block-like specimen under different loading conditions, see also figure 2, namely

- (i) section 4.1: rate-independent behaviour under cyclic electrical loading represented by a prescribed electric potential (linearly in- and decreased) at the top surface ϕ_{top}^p – the electric potential at the bottom surface ϕ_{bot}^p constantly being zero – is discussed. In addition compressive stresses in axial or lateral direction are uniformly applied to the top surface, $\mathbf{t}_{\text{top}}^p$, and, respectively, to the side surfaces $\mathbf{t}_{\text{sid}}^p$ – the bottom surface being throughout clamped.
- (ii) section 4.2: rate-dependent behaviour under cyclic electrical loading and axial compressive stresses are elaborated, compare (i).
- (iii) section 4.3: by analogy with (ii), rate-dependent behaviour under cyclic electrical loading and lateral compressive stresses (applied to the four pairwise opposite side surfaces) is investigated.

Since experimental measurements given in the literature are commonly referred to so-called integrated macroscopic data, we apply a simple volume averaging technique to the results obtained from three-dimensional finite element simulations. Moreover, contributions of interest are projected onto the (macroscopic) axial direction, \mathbf{e}_3 say, so that typical hysteresis and butterfly curves are determined by the scalar-valued quantities

$$\begin{aligned} D &= \frac{1}{\mathcal{V}} \int_{\mathcal{V}} \mathbf{D} \cdot \mathbf{e}_3 \, \forall, \\ E &= \frac{1}{\mathcal{V}} \int_{\mathcal{V}} \mathbf{E} \cdot \mathbf{e}_3 \, \forall, \\ e &= \frac{1}{\mathcal{V}} \int_{\mathcal{V}} \mathbf{e}_3 \cdot \boldsymbol{\varepsilon} \cdot \mathbf{e}_3 \, \forall. \end{aligned} \quad (14)$$

All numerical examples studied in the following refer to a block-like $9 \times 9 \times 9$ specimen, whereby the discretisation is performed with $9 \times 9 \times 9$ eight node bricks (Q1Q1); see figure 2 for a schematic illustration. Further studies concerning influences of the chosen mesh – and load step size are highlighted in Arockiarajan, Menzel, Delibas, and Seemann (2006b) but not addressed in this contribution. In view of material parameters, representative PZT 51 values have been adopted from the literature: $k = 0.0666$ [μ F/m], $d_{33} = 1.52 \times 10^{-9}$ [m/V], $d_{31} = -0.57 \times 10^{-9}$ [m/V], $d_{15} = 1.856 \times 10^{-9}$ [m/V], Young's modulus $E = \mu [3\lambda + 2\mu] / [\lambda + \mu] = 30.3$ [GPa], Poisson ratio $\nu = \lambda / [2\lambda + 2\mu] = 0.3$, $\boldsymbol{\varepsilon}^s = 2.7 \times 10^{-3}$ $P^s = P_0 = 0.1938$ [C/m²], $E_0 = 0.4$ [MV/m], and, moreover, $C_1 = 0.00325$ [MV s/m] and $C_2 = 0.00325$ [MPa s] (both ‘per unit thickness’) as well as $|\Delta\phi_{\text{top}}^p| = 1.0$ [KV]. Three different loading frequencies and amplitudes are taken into account, namely $f_\phi = 0.01$, $f_\phi = 0.10$, $f_\phi = 1.00$ [Hz] and $\hat{E} = 2.0$, $\hat{E} = 1.5$, $\hat{E} = 1.0$ [MV/m]. The parameter entering the modelling of intergranular effects is chosen throughout as $p = 5$, unless otherwise stated.

4.1 Rate-independent behaviour

To set the stage and for reasons of comparison with experimental data reported by Fang and Li (1999), the simulation of rate-independent material behaviour is first addressed in this section. Practically speaking, the volume fraction parameter τ , as introduced in eqs.(10, 11), is a priori set identical to one. Figures 3 and 4 show the classical hysteresis loop (electric displacement D versus electric field E) and butterfly curve (total strains e versus electric field E), whereby no additional stresses have been superimposed. Within the computations shown in figure 3 the switching

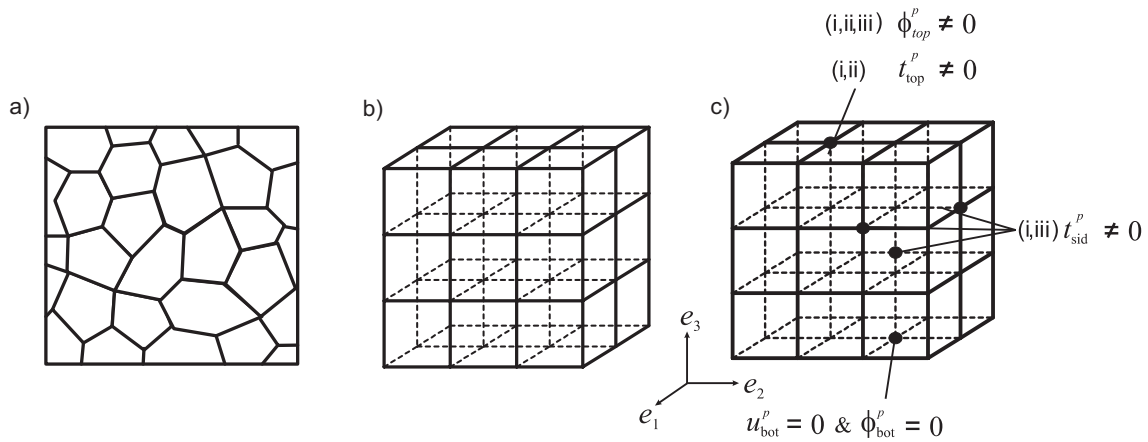


Figure 2: Two-dimensional graphical representation of a natural assembly of grains (a), schematic three-dimensional finite element discretisation (b), and illustration of the applied boundary conditions (c).

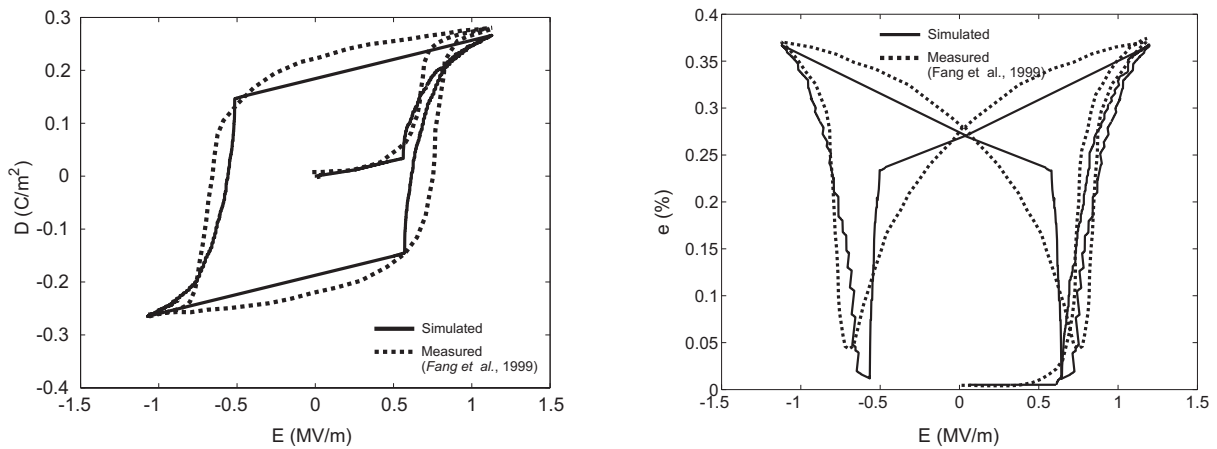


Figure 3: Hysteresis and butterfly curves under quasi-static loading without probabilistic approach ($p = 0$) and without additional superimposed stresses.

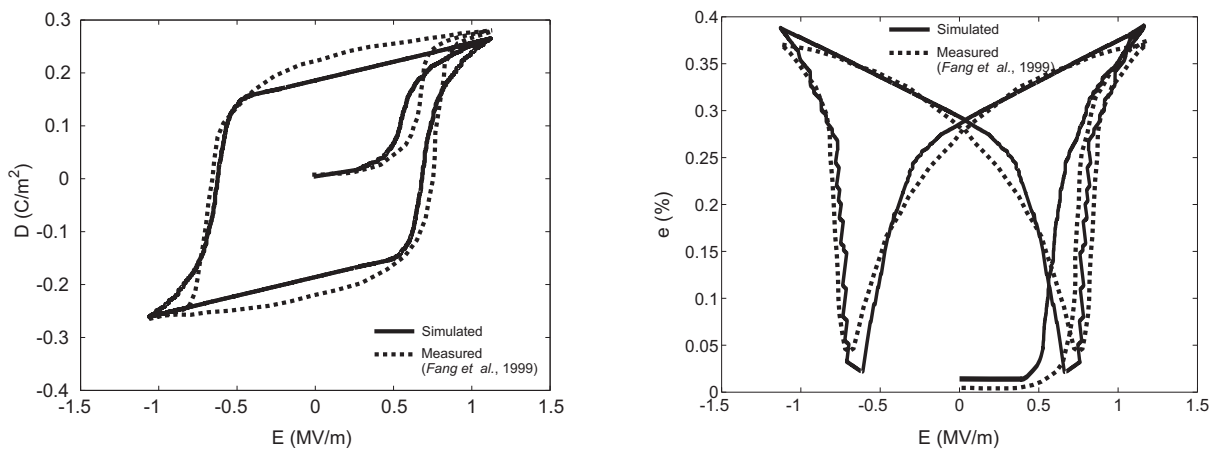


Figure 4: Hysteresis and butterfly curves under quasi-static loading with probabilistic approach ($p = 5$) but without additional superimposed stresses.

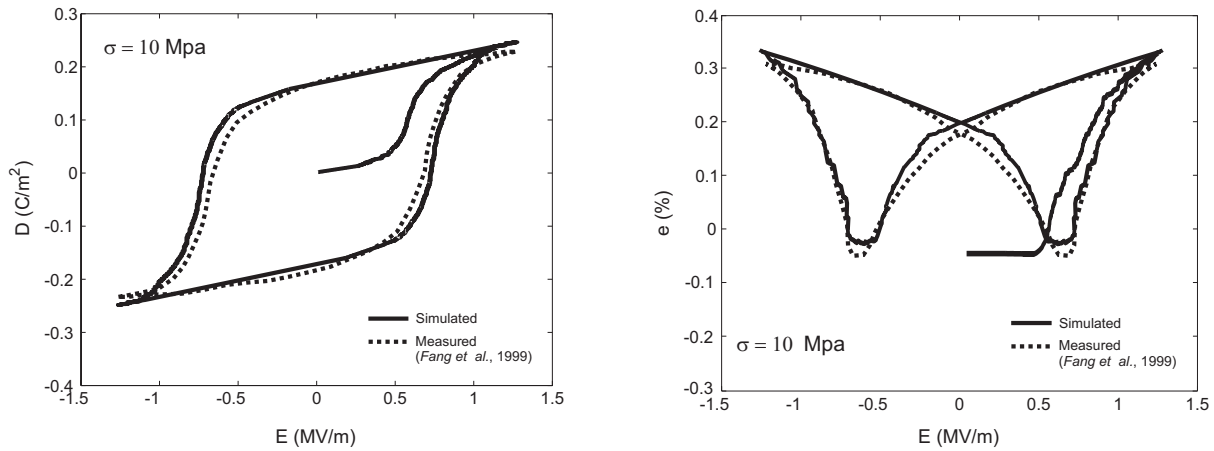


Figure 5: Hysteresis and butterfly curves under quasi-static loading with axial compressive stresses $\sigma = 10$ MPa.

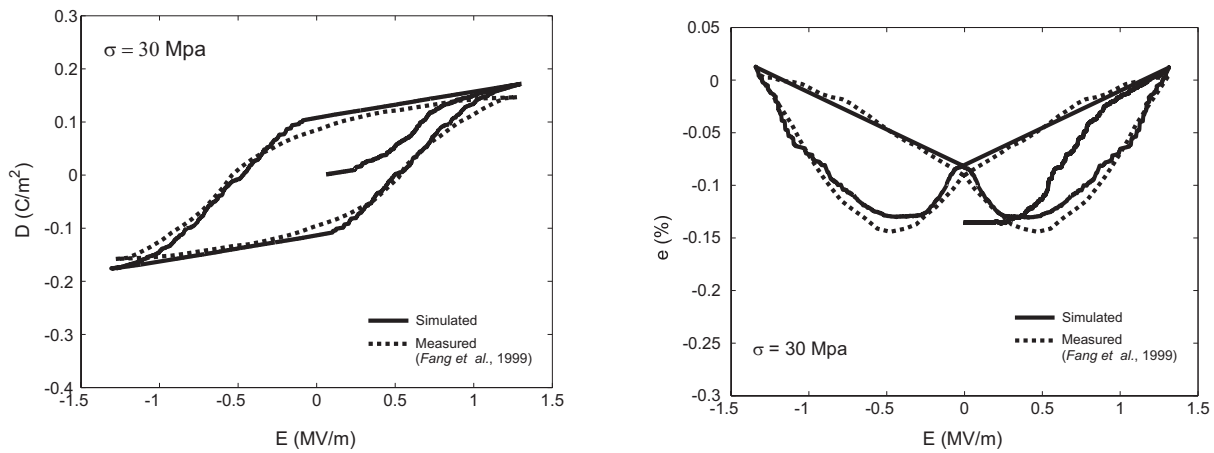


Figure 6: Hysteresis and butterfly curves under quasi-static loading with axial compressive stresses $\sigma = 30$ MPa.

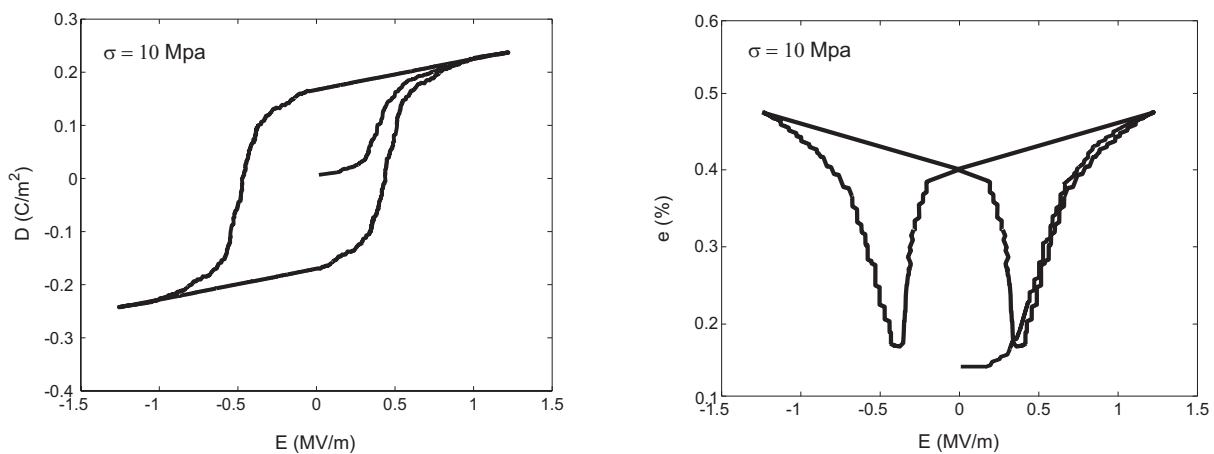


Figure 7: Hysteresis and butterfly curves under quasi-static loading with lateral compressive stresses $\sigma = 10$ MPa.

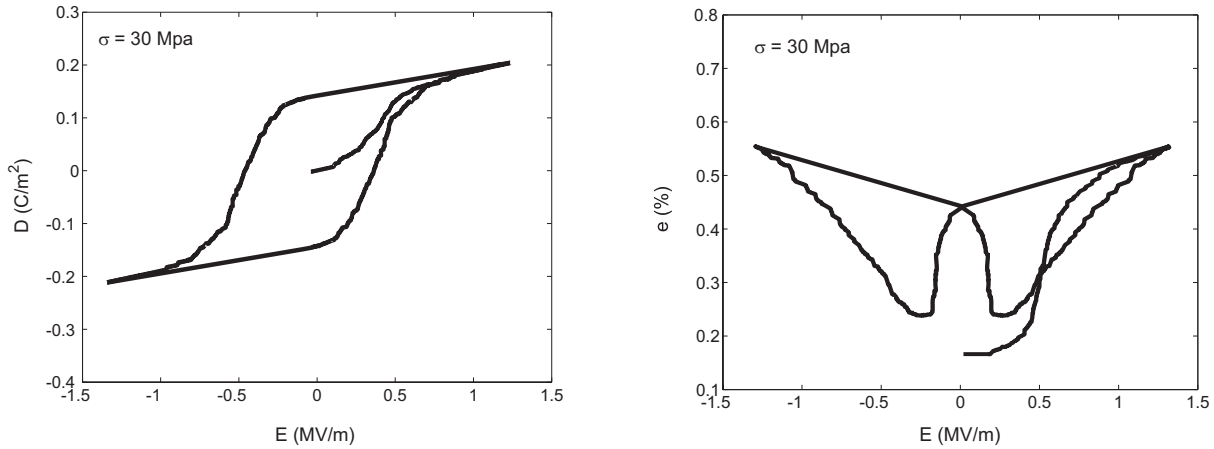


Figure 8: Hysteresis and butterfly curves under quasi-static loading with lateral compressive stresses $\sigma = 30$ MPa.

probability function has been neglected by setting $p = 0$. It is clearly seen that the hysteresis and butterfly curves possess sharp corners near the macroscopic coercive electric field which is not observed in experiments. Due to the incorporation of grain boundary effects by means of the probabilistic ansatz in eq.(12), the obtained graphs proceed rather smooth near the macroscopic coercive electric field parameter so that better agreement with experimental measurements performed by Fang and Li (1999) is observed.

The effects of axial compressive stresses on hysteresis and butterfly curves are highlighted in figures 5 and 6, whereby different loading levels are addressed, namely 10 and 30 MPa. Compared to the results displayed in figure 4, the switching range is enlarge under axial compressive stresses. Since two successive 90° switching processes are preferred to one 180° transformation, a reduction of the macroscopic coercive electric field is experimentally observed and also reflected by our numerical results. Similarly, a reduction of the saturation polarisation value occurs. In addition, figures 5 and 6 clearly monitor that both, the hysteresis as well as the butterfly curves ‘flatten’ when increasing the compressive stresses. Moreover, the macroscopic (projected) strain level shifts towards compression – to give an example, $e|_{E=0} < 0$ for, e.g., $\sigma = 30$ MPa.

By analogy with figures 5 and 6, rate-independent behaviour under lateral compressive stresses is

addressed in figures 7 and 8. Compared to figure 4, an expanded switching range is noted and, similar to figures 5 and 6, a reduced macroscopic coercive electric field as well as an increased saturation polarisation magnitude are observed. However, both, the hysteresis and butterfly curves turn out to be ‘compacted in horizontal direction’ under lateral compressive stresses. Nevertheless, the butterfly curves also ‘flatten’ for the considered boundary conditions so that the critical level for domain switching increases with increasing mechanical loading.

4.2 Rate-dependent behaviour under axial compressive stresses

In this section, rate-dependent properties are studied under axial compressive stresses – figures 9 to 14 show hysteresis and butterfly curves for various loading amplitudes ($\hat{E} = 2.0, 1.5, 1.0$ MV/m) and frequencies ($f_\phi = 0.01, 0.10, 1.00$ Hz).

As expected, a reduction in the macroscopic coercive electric field and the saturation polarisation value is observed under axial compressive stresses irrespective of the applied loading frequencies. Moreover, the macroscopic (projected) total strains shift towards the compressive regime. The numerical results highlighted in figures 9 to 14 underpin that the macroscopic coercive electric field value strongly depends on the applied loading frequency. Practically speaking, an increase of the coercive electric field is observed

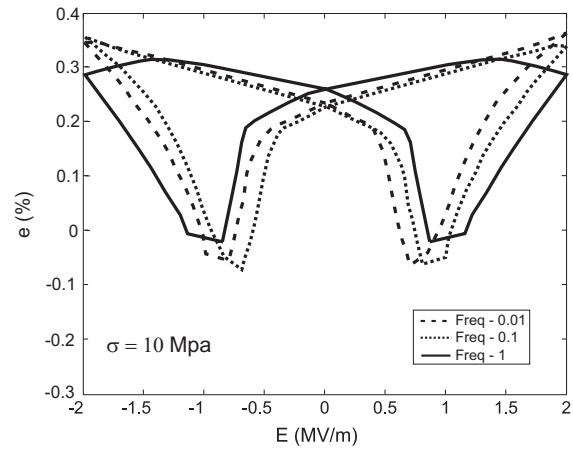
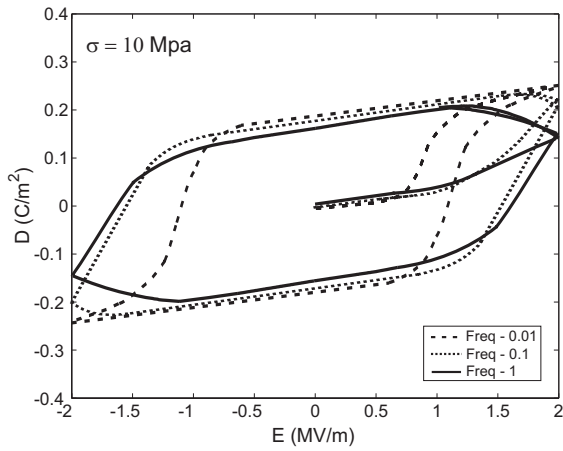


Figure 9: Hysteresis and butterfly curves under axial compressive stresses $\sigma = 10$ MPa for $\hat{E} = 2.0$ MV/m.

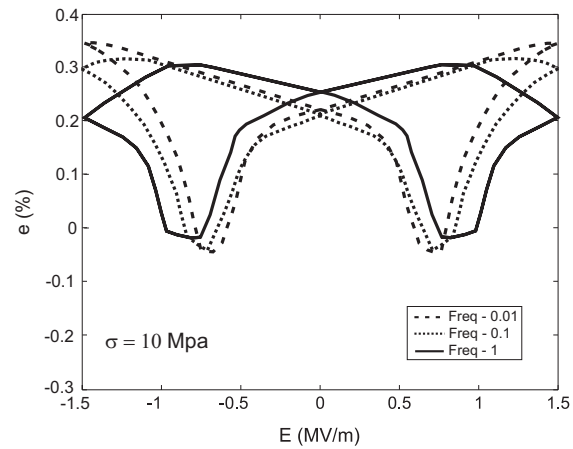
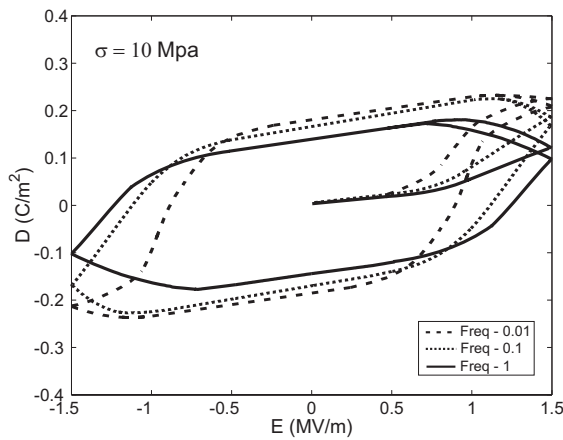


Figure 10: Hysteresis and butterfly curves under axial compressive stresses $\sigma = 10$ MPa for $\hat{E} = 1.5$ MV/m.

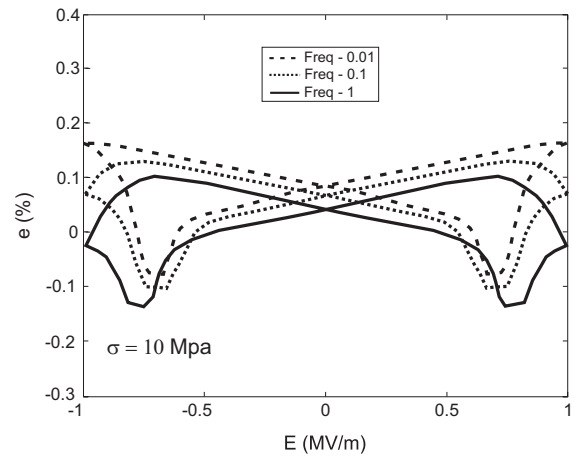
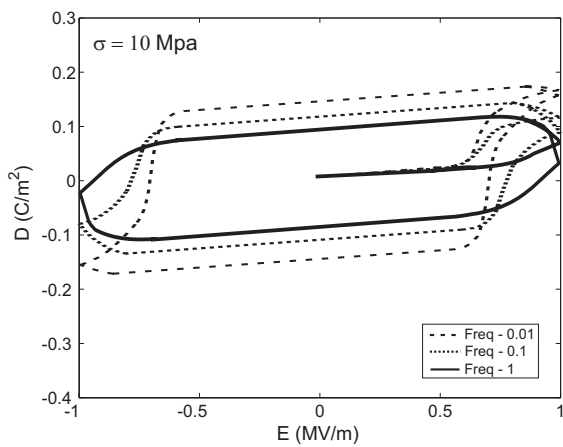


Figure 11: Hysteresis and butterfly curves under axial compressive stresses $\sigma = 10$ MPa for $\hat{E} = 1.0$ MV/m.

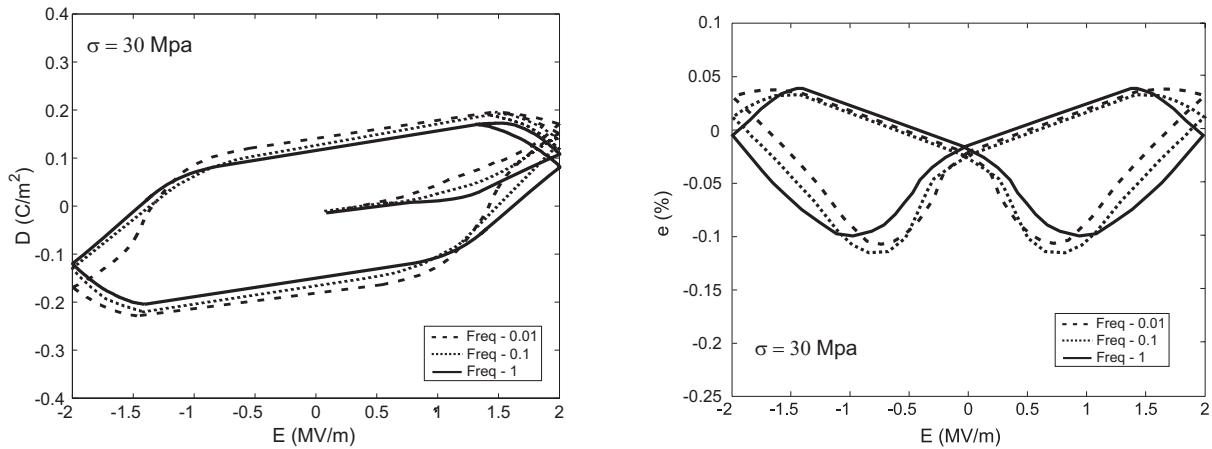


Figure 12: Hysteresis and butterfly curves under axial compressive stresses $\sigma = 30$ MPa for $\hat{E} = 2.0$ MV/m.

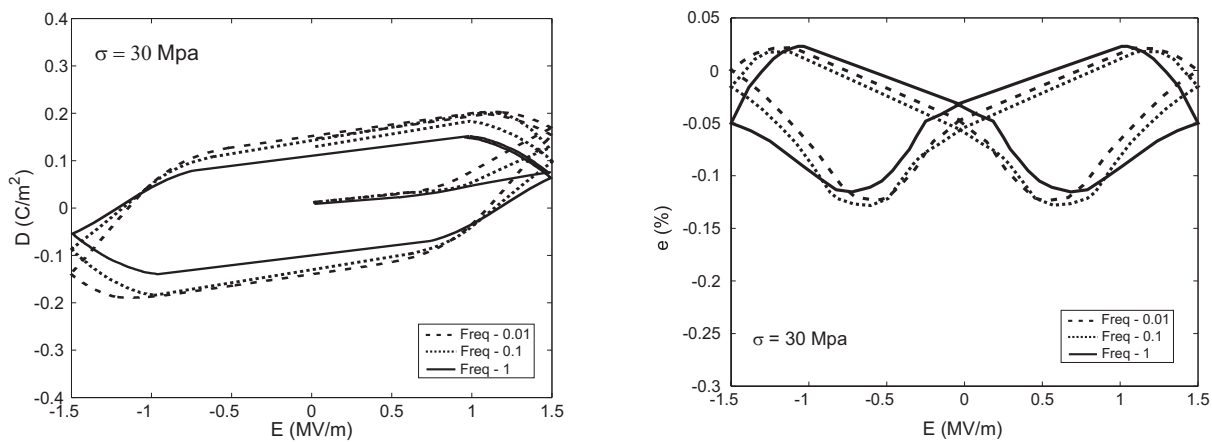


Figure 13: Hysteresis and butterfly curves under axial compressive stresses $\sigma = 30$ MPa for $\hat{E} = 1.5$ MV/m.

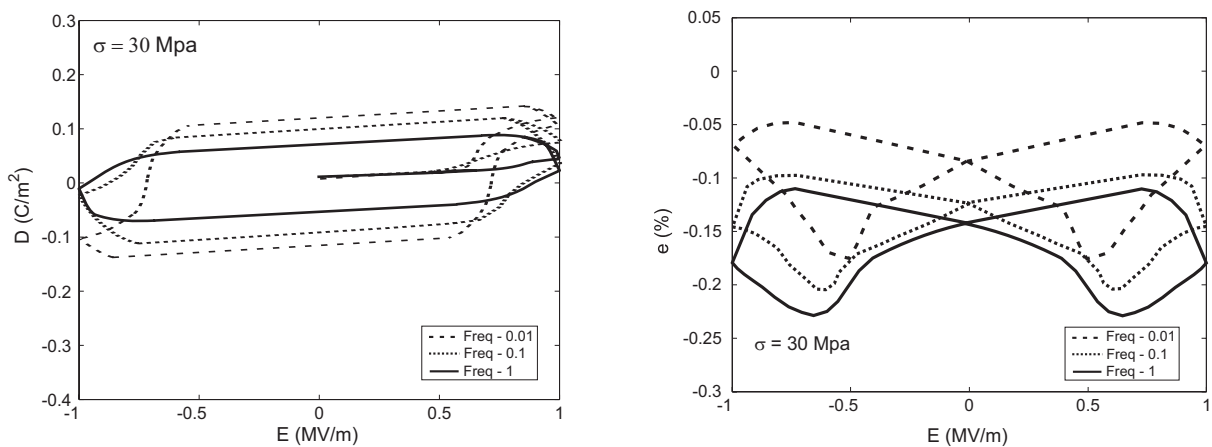


Figure 14: Hysteresis and butterfly curves under axial compressive stresses $\sigma = 30$ MPa for $\hat{E} = 1.0$ MV/m.

when raising the loading frequency f_ϕ . Similar effects are obtained for amplified load levels \hat{E} . For the results displayed in figures 11 and 14, the loading amplitude $\hat{E} = 1.0$ [MV/m] is close to the macroscopic coercive electric field value itself – however, even within this regime the coercive fields vary depending on the applied loading frequency. Furthermore, it is clearly seen that both, the electric displacements as well as the longitudinal strains decrease for higher loading frequencies for all applied electrical loading amplitudes. As an interesting aspect, the electric displacements and total strains in figure 10 and 11 are, say, not saturated for all chosen loading scenarios so that an increase of these quantities upon reverse loading takes place. From figures 9, 10, 12, and 13 one can additionally conclude that the remanent polarisation value (electrical displacement at zero electric field) and remanent strains (longitudinal strains at zero electric field) are not varying significantly for loading frequencies f_ϕ of 0.01 and 0.10 Hz at maximum amplitudes of the macroscopic electric field \hat{E} of 2.0 and 1.5 MV/m. Finally, note that the remanent polarisation as well as the remanent strains decrease for increasing loading frequency at a loading amplitude of $\hat{E} = 1.0$ MV/m; compare figures 11 and 14.

4.3 Rate-dependent behaviour under lateral compressive stresses

In this section, rate-dependent properties are studied under lateral compressive stresses – figures 15 to 20 show hysteresis and butterfly curves for various loading amplitudes ($\hat{E} = 2.0, 1.5, 1.0$ MV/m) and frequencies ($f_\phi = 0.01, 0.10, 1.00$ Hz). As a conclusion, lateral compressive stress yield a reduction in the macroscopic coercive electric field and an increase in the saturation polarisation value irrespective of the considered loading frequencies. Contrary to the elaboration in section 4.2, the macroscopic strain level does not move towards overall compressive values under lateral compressive stresses. The results displayed in this section highlight hysteresis and butterfly curves which are rather ‘squeezed in horizontal direction’ compared to those obtained for axial compressive stresses. Furthermore, lower loading

frequencies result in decreasing coercive electric fields. By analogy with section 4.2, figures 16 and 19 show that the electric displacements and the total strains at maximum loading amplitudes are not saturated for a loading frequencies of, for instance, 1.00 Hz as compared to the almost quasi-static cases at $f_\phi = 0.01$ or $f_\phi = 0.1$ Hz. Moreover, the remanent polarisation value increases when decreasing the loading frequency.

5 Summary

A micro-mechanically motivated model, embedded into a robust three-dimensional coupled finite element formulation, has been reviewed in this contribution. The main goal of this work, however, was to apply the proposed computation framework to various boundary value problems, namely rate-dependent response under axial and lateral compressive stresses. Switching processes have thereby been initiated by means of an energy-based criterion. Furthermore, a linear kinetics theory together with a simple volume fraction concept has been applied to model the propagation of switching processes. As a key aspect, grain boundary effects were incorporated via a probabilistic approach in terms of a polynomial ansatz. As a first step, each finite element was assumed to represent one grain so that no precise distinction between grains and domains has been made. The initially un-poled virgin state of the bulk material was incorporated by means of a randomly generated initial polarisation directions of individual elements. The adopted model for piezoelectric materials has been embedded into a finite element formulation, whereby switching phenomena have been realised via a simple and robust staggered iteration technique. Finally, straightforward volume averaging enables to study the overall macroscopic behaviour represented via commonly used and experimentally identified hysteresis and butterfly curves. The numerically obtained results predicted important insights into nonlinear rate-dependent effects of piezoelectric materials. Due to the lack of experimental data available in the literature, the simulations were solely compared with measurements for the rate-independent case.

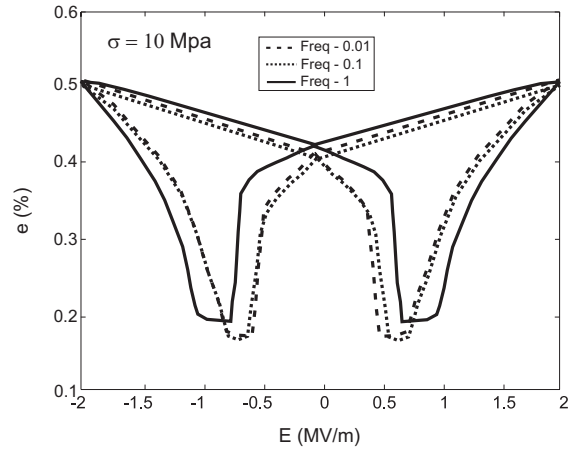
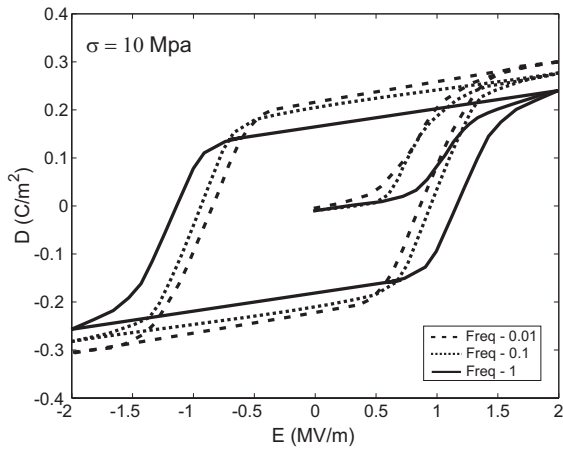


Figure 15: Hysteresis and butterfly curves under lateral compressive stresses $\sigma = 10$ MPa for $\hat{E} = 2.0$ MV/m.

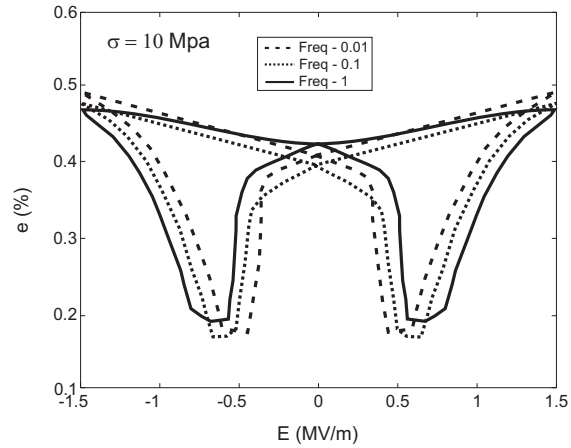
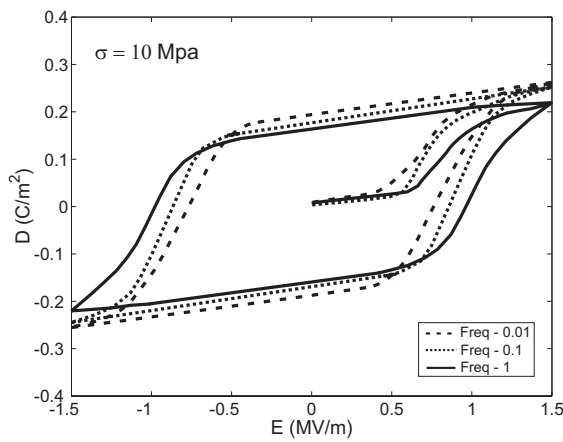


Figure 16: Hysteresis and butterfly curves under lateral compressive stresses $\sigma = 10$ MPa for $\hat{E} = 1.5$ MV/m.

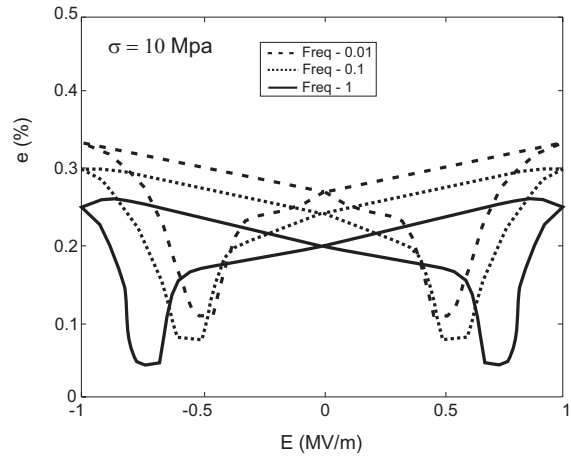
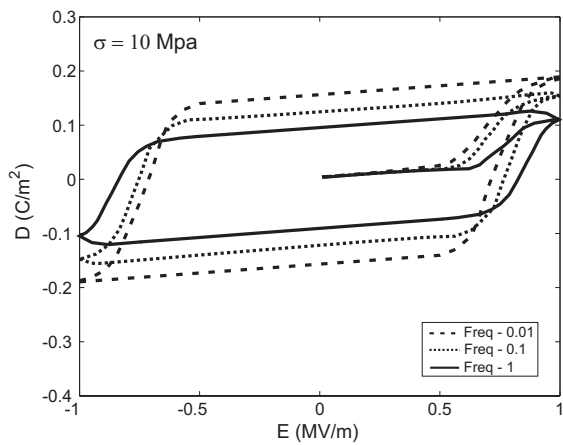


Figure 17: Hysteresis and butterfly curves under lateral compressive stresses $\sigma = 10$ MPa for $\hat{E} = 1.0$ MV/m.

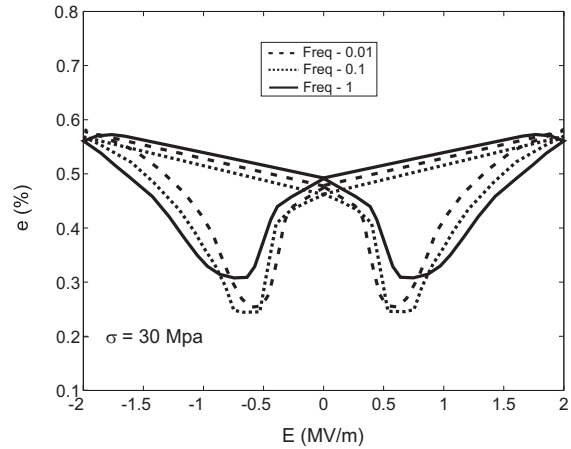
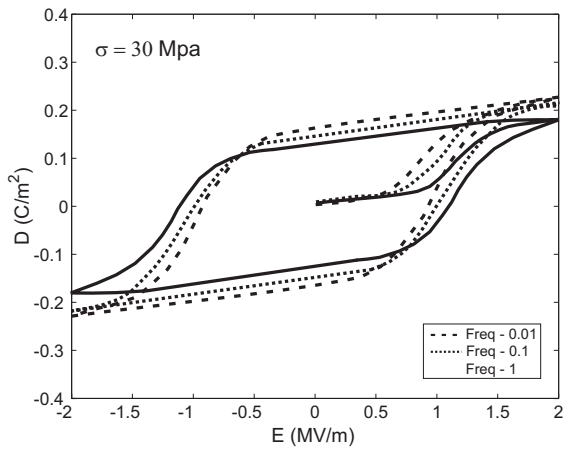


Figure 18: Hysteresis and butterfly curves under lateral compressive stresses $\sigma = 30$ MPa for $\hat{E} = 2.0$ MV/m.

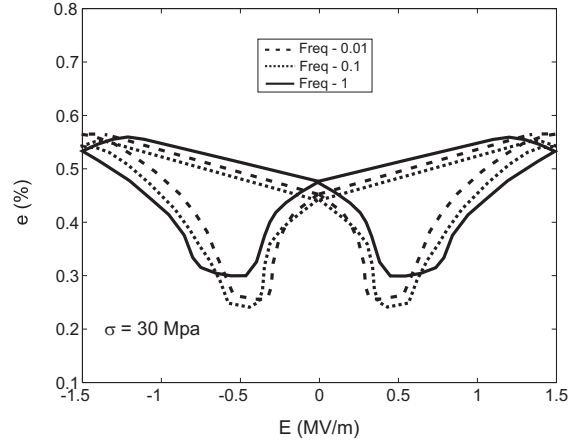
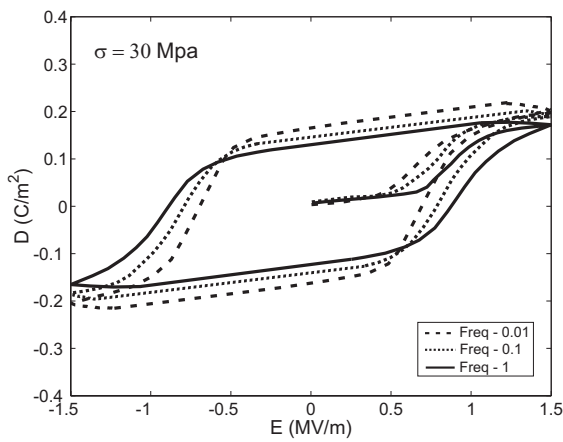


Figure 19: Hysteresis and butterfly curves under lateral compressive stresses $\sigma = 30$ MPa for $\hat{E} = 1.5$ MV/m.

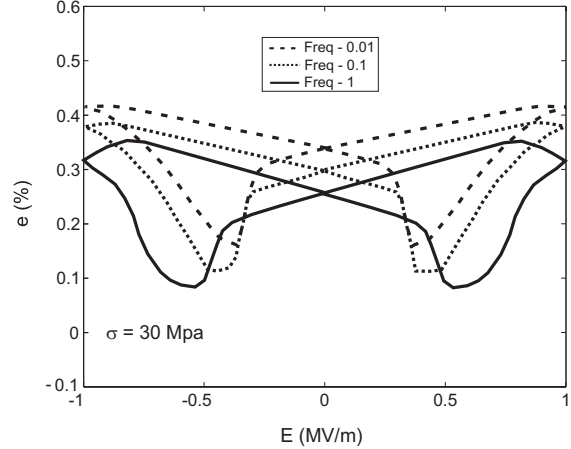
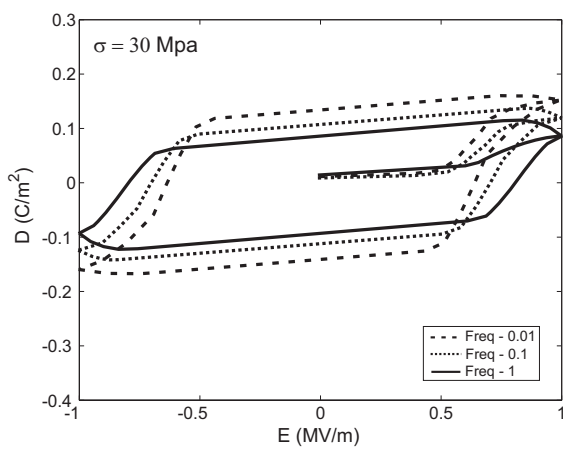


Figure 20: Hysteresis and butterfly curves under lateral compressive stresses $\sigma = 30$ MPa for $\hat{E} = 1.0$ MV/m.

References

- Abeyaratne, R.; Kim, S. J.; Knowles, J. K.** (1994): One dimensional model for shape memory alloys. *Int. J. Solids Struct.*, vol. 31, pp. 2229–2249.
- Allik, H.; Hughes, T. J. R.** (1970): Finite element method for piezoelectric vibration. *Int. J. Numer. Methods Engng.*, vol. 2, pp. 151–157.
- Arlt, G.** (1996a): A physical model for hysteresis curves of ferroelectric ceramics. *Ferroelectrics*, vol. 189, pp. 103–119.
- Arlt, G.** (1996b): Switching and dielectric non-linearity of ferroelectric ceramics. *Ferroelectrics*, vol. 189, pp. 91–101.
- Arlt, G.** (1997): A model for switching and hysteresis in ferroelectric ceramics. *Integrated Ferroelectrics*, vol. 16, pp. 229–236.
- Arockiarajan, A.; Delibas, B.; Menzel, A.; Seemann, W.** (2006): Studies on rate dependent switching effects of piezoelectric materials using a finite element model. *Comput. Mater. Sci.*, vol. 37, pp. 306–317.
- Arockiarajan, A.; Menzel, A.; Delibas, B.; Seemann, W.** (2006a): Computational modeling of rate-dependent domain switching in piezoelectric materials. *Euro. J. Mech. A/Solids*, vol. 25, pp. 950–964.
- Arockiarajan, A.; Menzel, A.; Delibas, B.; Seemann, W.** (2006b): Micromechanical modeling of switching effects in piezoelectric materials - a robust coupled finite element approach. *J. Intelligent Mat. Sys. Struct.* in press.
- Bassiouny, E.; Ghaleb, A. F.; Maugin, G. A.** (1988a): Thermodynamical formulation for coupled electromechanical hysteresis effects - I. basic equations. *Int. J. Engng. Sci.*, vol. 26, no. 12, pp. 1279–1295.
- Bassiouny, E.; Ghaleb, A. F.; Maugin, G. A.** (1988b): Thermodynamical formulation for coupled electromechanical hysteresis effects - II. poling of ceramics. *Int. J. Engng. Sci.*, vol. 26, no. 12, pp. 1297–1306.
- Cao, H.; Evans, A. G.** (1993): Nonlinear deformation of ferroelectric ceramics. *J. Amer. Ceramic Soc.*, vol. 76, pp. 890–896.
- Chen, W.; Lynch, C. S.** (1998): A micro-electro-mechanical model for polarization switching of ferroelectric materials. *Acta Mater.*, vol. 46, pp. 5303–5311.
- Delibas, B.; Arockiarajan, A.; Seemann, W.** (2006): Rate dependent properties of perovskite type tetragonal piezoelectric materials using micromechanical model. *Int. J. Solids Struct.*, vol. 43, pp. 697–712.
- Elhadrouz, M.; Zineb, T. B.; Patoor, E.** (2005): Constitutive law for ferroelectric and ferroelastic single crystals: a micromechanical approach. *Comput. Mater. Sci.*, vol. 32, pp. 355–359.
- Fang, D.; Li, C.** (1999): Nonlinear electro-mechanical behavior of a soft PZT-51 ferroelectric ceramic. *J. Mat. Sci.*, vol. 34, pp. 4001–4010.
- Gaudenzi, P.; Bathe, K. J.** (1995): An iterative finite element procedure for the analysis of piezoelectric continua. *J. Intelligent Mat. Sys. Struct.*, vol. 6, pp. 266–273.
- Goldstein, H.; Poole, C.; Safko, J.** (2002): *Classical Mechanics*. Addison Wesley, New York.
- Huber, J. E.; Fleck, N. A.** (2004): Ferroelectric switching: a micromechanics model versus measured behaviour. *Euro. J. Mech. A/Solids*, vol. 23, pp. 203–217.
- Hwang, S. C.; Lynch, C. S.; McMeeking, R. M.** (1995): Ferroelectric/ferroelastic interactions and a polarization switching model. *Acta Metal. Mater.*, vol. 5, pp. 2073–2084.
- Hwang, S. C.; McMeeking, R. M.** (1998a): A finite element model of ferroelectric polycrystals. *Ferroelectrics*, vol. 211, pp. 177–194.
- Hwang, S. C.; McMeeking, R. M.** (1998b): The prediction of switching in polycrystalline ferroelectric ceramics. *Ferroelectrics*, vol. 207, pp. 465–495.

- Jaffe, B.; Cook, W. R.; Jaffe, H.** (1971): *Piezoelectric Ceramics*. Academic Press, London, New York.
- Janta, J.** (1971): The influence of the shape of domains on the ferroelectric hysteresis loop. *Ferroelectrics*, vol. 2, pp. 299–302.
- Kamlah, M.** (2001): Ferroelectric and ferroelastic piezoceramics-modeling of electromechanical hysteresis phenomena. *Continuum Mech. Thermodyn.*, vol. 13, no. 4, pp. 219–268.
- Kamlah, M.; Tsakmakis, C.** (1999): Phenomenological modeling of non-linear electromechanical coupling in ferroelectrics. *Int. J. Solids Struct.*, vol. 36, pp. 669–695.
- Kim, S. J.; Jiang, Q.** (2002): A finite element model for rate-dependent behavior of ferroelectric ceramics. *Int. J. Solids Struct.*, vol. 39, pp. 1015–1030.
- Kim, S. J.; Seelecke, S.** (2007): A rate-dependent three-dimensional free energy model for ferroelectric single crystals. *Int. J. Solids Struct.*, vol. 44, pp. 1196–1209.
- Landauer, R.; Young, D. R.; Drougard, M. E.** (1956): Polarization reversal in the barium titanate hysteresis loop. *J. Appl. Phys.*, vol. 27, pp. 752–758.
- Landis, C. M.** (2002): Fully coupled, multi-axial, symmetric constitutive laws for polycrystalline ferroelectric ceramics. *J. Mech. Phys. Solids*, vol. 50, pp. 127–152.
- Liu, T.; Lynch, C. S.** (2006): Orientation dependence of nonlinearity and hysteresis in PZN-4.5%PT single crystals, II: bipolar electromechanical response. *J. Intelligent Mat. Sys. Struct.*, vol. 17, pp. 931–937.
- Lu, W.; Fang, D. N.; Li, C. Q.; Hwang, K. C.** (1999): Nonlinear electric-mechanical behaviour and micromechanics modeling of ferroelectric domain evolution. *Acta Mater.*, vol. 47, pp. 2913–2926.
- Lupascu, D. C.** (2004): *Fatigue in Ferroelectric Ceramics and Related Issues*. Springer, Heidelberg.
- Lynch, C. S.** (1996): The effect of uniaxial stress on the electro-mechanical response of 8/65/35 PLZT. *Acta Mater.*, vol. 44, pp. 4137–4148.
- Lynch, C. S.; McMeeking, R. M.** (1994): Finite strain ferroelectric constitutive laws. *Ferroelectrics*, vol. 160, pp. 177–184.
- McMeeking, R. M.; Hwang, S. C.** (1997): On the potential energy of a piezoelectric inclusion and the criterion for ferroelectric switching. *Ferroelectrics*, vol. 200, pp. 151–173.
- Merz, W. J.** (1954): Domain formation and domain wall motions in ferroelectric BaTiO₃ single crystals. *Phys. Rev.*, vol. 95, no. 3, pp. 690–698.
- Omura, M.; Adachi, H.; Ishibashi, Y.** (1991): Simulation of ferroelectrics characteristics using a one-dimensional lattice model. *Japanese J. Appl. Phys.*, vol. 30, pp. 2384–2387.
- Schröder, J.; Gross, D.** (2004): Invariant formulation of the electromechanical enthalpy function of transversely isotropic piezoelectric materials. *Arch. Appl. Mech.*, vol. 73, pp. 533–552.
- Schröder, J.; Romanowski, H. C.** (2005): A thermodynamically consistent mesoscopic model for transversely isotropic ferroelectric ceramics in a coordinate-invariant setting. *Arch. Appl. Mech.*, vol. 74, pp. 863–877.
- Smith, R. C.** (2005): *Smart material systems – Model development*. Society of Industrial and Applied Mathematics, Philadelphia.
- Smith, R. C.; Ounates, Z.** (2000): A domain wall model for hysteresis in piezoelectric materials. *J. Intelligent Mat. Sys. Struct.*, vol. 11, pp. 62–79.
- Srivastava, N.; Weng, G. J.** (2006): A dual-phase homogenization theory for the hysteresis and butterfly-shaped behavior of ferroelectric single crystals. *Mechanics of Materials*, vol. 38, pp. 945–957.

Sun, C. T.; Achuthan, A. (2004): Domain-switching criteria for ferroelectric materials subjected to electrical and mechanical loads. *J. Amer. Ceramic Soc.*, vol. 87, pp. 395–400.

Uchino, K. (1997): *Piezoelectric Actuators and Ultrasonic Motors*. Kluwer Academic Publishers, Boston.

Viehland, D.; Chen, Y.-H. (2000): Random-field model for ferroelectric domain dynamics and polarization reversal. *J. Appl. Phys.*, vol. 88, pp. 6696–6707.

Zhou, D.; Kamlah, M.; Munz, D. (2001): Rate dependence of soft PZT ceramics under electric field loading. In *Proc. SPIE 4333*, pp. 64–70.